

| REPORT DOCUMENTATION PAGE   |   |   | Form Approved<br>OMB No. 0704-0188                                       |  |
|---|---|---|--|--|
| <small>Public reporting burden for this collection of information is estimated to average 1 hour per response, including the time for reviewing instructions, searching existing data sources, gathering and maintaining the data needed, and completing and reviewing the collection of information. Send comments regarding this burden estimate or any other aspect of this collection of information, including suggestions for reducing this burden, to Washington Headquarters Services, Directorate for Information Operations and Reports, 1215 Jefferson Davis Highway, Suite 1204, Arlington, VA 22202-4302, and to the Office of Management and Budget, Paperwork Reduction Project (0704-0188), Washington, DC 20503.</small>   |   |   |  |  |
| 1. AGENCY USE ONLY (Leave blank)  |   | 2. REPORT DATE<br>Sept. 12, 1994                        |  | 3. REPORT TYPE AND DATES COVERED<br>Interim Technical Report 7/15/93-7/14/94 |
| 4. TITLE AND SUBTITLE<br>High Gain, Low Noise and Broadband Raman and Brillouin Fiber -Optic Amplifiers, Channel Selectors and Switches   |   |   | 5. FUNDING NUMBERS<br>DAAL03-91-G-0301                                   |  |
| 6. AUTHOR(S)<br>Chung Yu  |   |   |  |  |
| 7. PERFORMING ORGANIZATION NAME(S) AND ADDRESS(ES)<br>North Carolina A & T State University<br>Greensboro, NC 27411   |   |   | PERFORMING ORGANIZATION<br>REPORT NUMBER                                 |  |
| 9. SPONSORING/MONITORING AGENCY NAME(S) AND ADDRESS(ES)<br>U. S. Army Research Office<br>P. O. Box 12211<br>Research Triangle Park, NC 27709-2211   |   |   | 10. SPONSORING/MONITORING<br>AGENCY REPORT NUMBER<br>ARO 28653, 1-EL-JAH |  |
| 11. SUPPLEMENTARY NOTES<br>The view, opinions and/or findings contained in this report are those of the author(s) and should not be construed as an official Department of the Army position, policy, or decision, unless so designated by other documentation.   |   |   |  |  |
| 12a. DISTRIBUTION/AVAILABILITY STATEMENT<br><br>Approved for public release; distribution unlimited.  |   |   | 12b. DISTRIBUTION CODE   |  |
| 13. ABSTRACT (Maximum 200 words)<br><p>Stimulated Brillouin and Raman scattering has been studied at 10.6 <math>\mu\text{m}</math> wavelength in fibers without much success due to the lack of low-loss, single-mode fibers and lasers with sufficiently narrow linewidth. The Brillouin based technology has advanced significantly with the advent of low-loss, single-mode fibers at 1.55 and 1.310 <math>\mu\text{m}</math> wavelengths. Conclusive experimental evidence points to the narrowband nature of Brillouin amplifiers, and redirects interest in their application to sensor and switching applications. Both stimulated Brillouin backscattering and guided acoustic wave forward scattering have been observed in fibers and are being explored for practical application as sensors to be bonded to or embedded in structures to monitor structural integrity. The stimulated Brillouin fiber ring laser is also being studied for its optical switching capabilities. The capability of this unique sensing mechanism is demonstrated in this report.</p> <p style="text-align: right;">DTIC QUALITY INSPECTED 4</p> |   |   |  |  |
| 14. SUBJECT TERMS<br>Brillouin Fiber Sensor, Structural Integrity, Optical Switching  |   |   | 15. NUMBER OF PAGES  |  |
|   |   |   | 16. PRICE CODE   |  |
| 17. SECURITY CLASSIFICATION OF REPORT<br>UNCLASSIFIED   | 18. SECURITY CLASSIFICATION<br>UNCLASSIFIED | 19. SECURITY CLASSIFICATION OF ABSTRACT<br>UNCLASSIFIED | 20. LIMITATION OF ABSTRACT<br>UL   |  |

19950202 067

**HIGH GAIN, LOW NOISE AND BROADBAND RAMAN  
AND BRILLOUIN FIBER-OPTIC AMPLIFIERS, CHANNEL  
SELECTORS AND SWITCHES**

**INTERIM TECHNICAL REPORT**

**CHUNG YU**

**7/15/93 - 7/14/94**

**U.S. ARMY RESEARCH OFFICE**

**DAAL03-91-G-0301**

**NORTH CAROLINA A&T STATE UNIVERSITY  
GREENSBORO, NC 27411**

Approved For Public Release;  
Distribution Unlimited.

|                    |  |
|--------------------|--|
| Accession For      |  |
| NTIS CRA&I         | <input checked="checked" type="checkbox"/> |
| DTIC TAB           | <input type="checkbox"/>                   |
| Unannounced        | <input type="checkbox"/>                   |
| Justification      |  |
| By                 |  |
| Distribution /     |  |
| Availability Codes |  |
| Dist               | Avail and / or<br>Special                  |
| A-1                |  |

## TABLE OF CONTENTS

|    |   |       |
|----|---|-------|
| 1. | Brillouin Scattering Based Sensor Survey        |       |
|    | SBS Experiments .....                           | 1-7   |
|    | GAWBS Theories and Experiments.....             | 7-13  |
| 2. | GAWBS Based Fiber Sensor Preliminary Tests..... | 14-20 |
| 4. | References.....                                 | 21    |
| 5. | Appendix  |       |
|    | GAWBS Theory .....                              | 22-24 |
|    | Acoustic Coupling to Fiber Theory.....          | 25-26 |

## 1. BRILLOUIN SCATTERING BASED SENSOR SURVEY

Optical fibers are generally considered to be passive devices; the light transmitted through them at reasonable power levels may be attenuated (or Rayleigh scattered) and reflected, but is not expected to be modulated. Conventional optical fiber sensors utilize the essential passivity of an unperturbed fiber to detect rather small perturbations externally imposed on the fiber.

Conventional passive fiber-is-the-sensor schemes fall into the following categories: interferometric, polarimetric, intensionmetric and modalmetric, utilizing the intrinsic phase, polarization and coherence of light and passive light guiding properties of the fiber, subjected to gross external mechanical perturbations, such as temperature, pressure, strain, corrosion, etc. These perturbations are assumed to translate directly into variations of fiber mechanical properties that affect light beam transmission. Such sensing is gross, and inherently incapable of distinguishing concurrent perturbations, such as temperature and pressure. Various versions of OTDR have also been explored for distributed temperature and strain sensing. However, the sensitivity of these systems is extremely low in standard fibers.

In an active fiber sensor based on stimulated Brillouin scattering, the interaction of light and excited vibrational modes is very different from Brillouin scattering in bulk media. The excitations in a fiber are the acoustic eigenmodes of the cylindrical structure rather than the plane waves of the Brillouin theory for bulk materials, and the acousto-optic interaction takes place in a confined geometry that relaxes the usual Bragg condition. As a result, the scattered light spectrum consists of dozens of lines, each corresponding to a different cylindrical mode rather than the two lines of the plane wave theory.

Stimulated Brillouin scattering (sBs), which is a stimulated backscattering phenomenon, and Guided Acoustic Wave Brillouin Scattering (GAWBS), which is essentially a forward scattering phenomenon, have basically the same stimulated scattering mechanism. The former is the result of strict adherence to the Bragg condition, while the latter is the consequence of relaxation of the Bragg condition. Hence, sBs always exists in any media (bulk or guiding structures, such as the fiber), while GAWBS occurs only in the confined geometry of the fiber.

SBS involves light scattering due to longitudinal phonons, while GAWBS is mainly due to near-resonant transverse acoustic waves in the fiber (see Appendix I).

Recently, sBs based active fiber optic sensors for temperature and strain have been reported while GAWBS fiber based sensing has not been extensively studied. Due to rising interest in this new sensing mechanism, it is timely to review the status of sBs and GAWBS sensor work to date. Such a status review on sBs sensors is given in Table 1. Since sBs theory is well established, only experimental schemes and data are highlighted in the table. We note, in particular, in the work of Bao and Kurashima that sensing fibers are excessively long, and two lasers are used; both these facts run counter to the principle of low cost and system simplicity. In an attempt to achieve single-laser operation, Duffy resorted to the use of polarization-maintaining, birefringent fibers in order to produce two sBs Stokes shifted backscattered light from the fast and slow axes of the fiber. Fiber length required is also reduced due to the small difference in the beat of the Stokes shifts from the two axes, rendering it detectable electronically by high sensitivity heterodyning. However, Duffy's data are still very tentative. We have detected sBs in our experiments and are now exploring the Duffy approach.

It is further noted that sBs temperature and strain sensing is inextricably inter-related, as demonstrated by Bao (Table 1). Thus, there is no means of extracting information on either one, if both are present. Furthermore, if the sBs sensor were to be used as a strain gauge on structures exposed to large ambient temperature fluctuations as in the case of installation on an aircraft, then calibration of the device is almost impossible. It is conceivable that such a device can serve as an ambient temperature sensor, when the fiber is suspended in a strain-free state. This device is thus theoretically single-measurand.

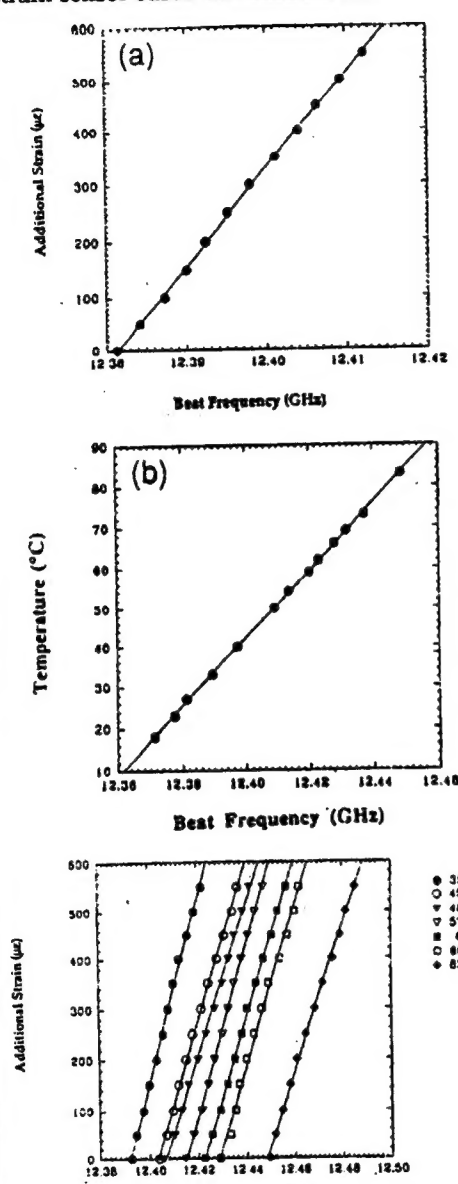
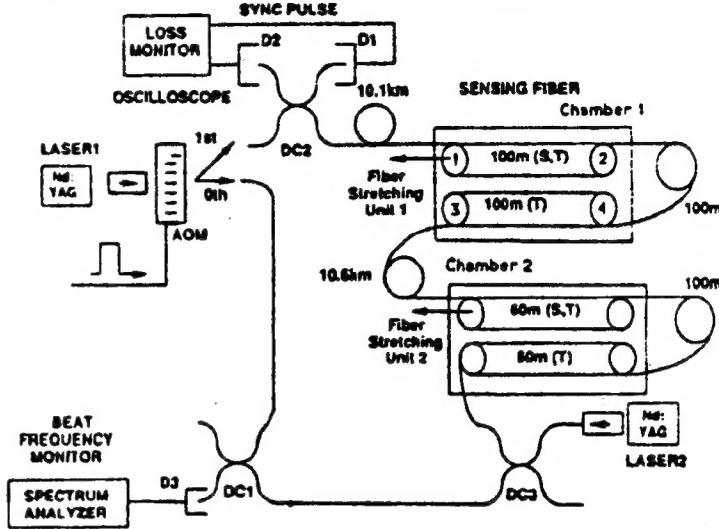
We have studied GAWBS extensively and have always observed the phenomenon at much lower incident laser powers and shorter fiber lengths as compared to the observation of sBs. This immediately connotes the potential superiority of the GAWBS sensor. To explore this fact in depth, the status of the GAWBS theory is revisited with additional confirmation from various viewpoints. A number of concepts are presented in Table 2.

This forward scattering mechanism has apparently been theorized and observed by a number of researchers. Their apparent divergent views are actually consistent when assembled, compared and properly interpreted. For instance, Stone attributed line broadening by Rayleigh-

Brillouin scattering, to diffraction by a finite aperture, which is the radius of the fiber. Based on fiber parameters and laser wavelength, he arrived at a maximum broadening of 500 MHz. Jen analyzed this phenomenon as acousto-optic interaction, arriving at the conclusion that only  $R_{0m}$ ,  $R_{2m}$ ,  $L_{0m}$ ,  $L_{2m}$ ,  $TR_{2m}$ , respectively radial (R), longitudinal (L) and torsional-radial acoustic modes are allowed. This is consistent with Shelby's and Marcuse's findings. Marcuse predicted depolarization of incident laser light in the fiber due to birefringence caused by periodic variations in the fiber diameter. Shelby derived formulas for the experimentally observed fiber acoustic eigenmodes with specific mode frequencies, which have been confirmed by Shiraki, us and others (see Table 3). The depolarizing  $TR_{2m}$  modes have been simulated graphically, showing the greatest amount of depolarizing scattering when the center of the fiber core becomes strongly elliptical (Table 5). We note the near absence of scattering by  $TR_{21}$ ,  $TR_{22}$ ,  $TR_{24}$ ,  $TR_{26}$ ; and high level of scattering by  $TR_{23}$ ,  $TR_{25}$ ,  $TR_{27}$  modes (see Table 4). Shelby also predicted extremely low TR mode scattering efficiency, leading us to call such low level scattering "noise". However, this readily observed "noise" over the strongly coherent sBs frequency shift is aptly explained by Corvo, who carried out an extensive spatial-temporal Fourier analysis of forward Brillouin scattering. He concluded theoretically that GAWBS would dominate over sBs for long pulse or cw lasers, and also correctly predicted the frequency shift increase with increasing diffraction angle, as observed by us. According to Table 3, Stone's line broadening formula is applied to Shelby, Shiraki and Yu experimental setups. The computed results are tabulated for comparison in Table 6. Maximum GAWBS bandwidth ranges from 900 MHz to about 400 MHz, agreeing reasonably with the data presented by the various groups.

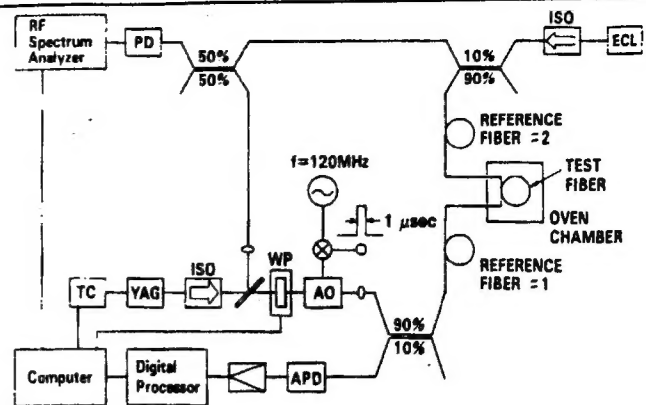
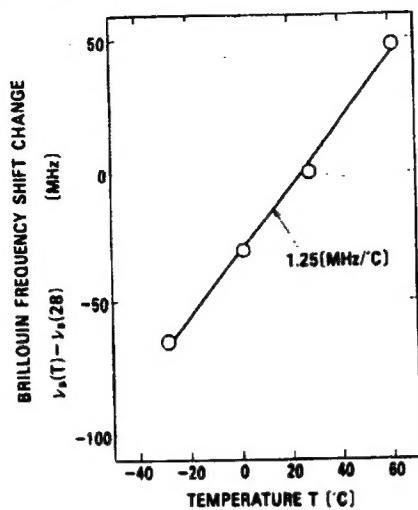
Dependence of sBs Stokes shift simultaneously on temperature and longitudinal strain is a severe drawback of this sensing process. On the other hand, a simple computation carried out in Table 6 clearly indicates the insensitivity of a GAWBS sensor to temperature and longitudinal strain. It is truly a structural integrity sensor. It has also occurred to us that since sBs involves backscattering of light and GAWBS involves forward scattered light, possibility exists of devising a single fiber system for sensing in both the forward and backward directions: backward sensing for temperature and longitudinal strain, and forward sensing for torsional-radial acoustic vibrations in the fiber, that reflect health of a structure to which the fiber is bonded. A setup for dual sensing is shown in Fig. 1. The sBs signal has been clearly observed by us as shown in Fig. 2.

Table 1: Available SBS Experimental Data As Sensing Mechanism

| Reference         | SBS   | Experimental Setup  |
|-------------------|---|---|
| <p>Bao (1994)</p> | <p><b>Purpose:</b> For distributed temperature and strain sensor based on Brillouin loss</p>  |  <p>Parameter:</p> <ul style="list-style-type: none"> <li>- Laser: Both lasers were solid-state cw diode pumped Nd:YAG ring lasers emitting close to 1319nm.</li> <li>- Max. Power: <math>\approx 10\text{mW}</math></li> <li>- Fiber length: 22km</li> </ul> |

Kurashima  
(1990)

**Purpose:** For distributed temperature sensors

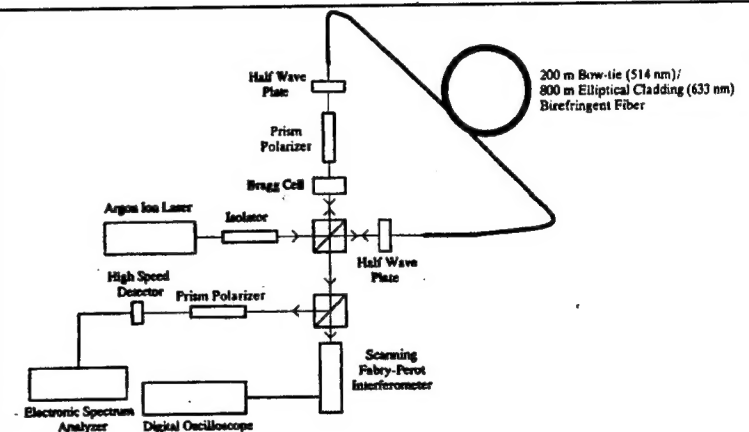
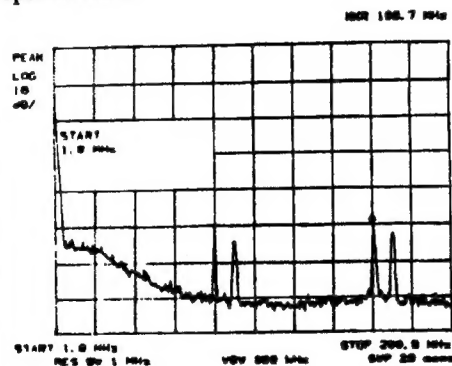


**Parameter:**

- Laser: Pump - 1.32 $\mu\text{m}$  frequency tunable Nd:YAG laser  
Probe - 1.32 $\mu\text{m}$  semiconductor laser
- Laser linewidth: Pump - 0.4MHz  
Probe - 1MHz
- Fiber length: 1.2km
- Fiber output: Pump - 1.8mW  
Probe - 0.3mW

Duffy  
(1993)

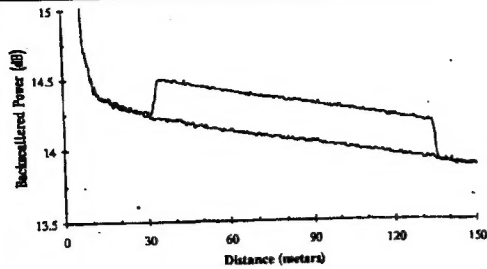
**Purpose:** Optical frequency shifter for sensing application using birefringent optical fiber.



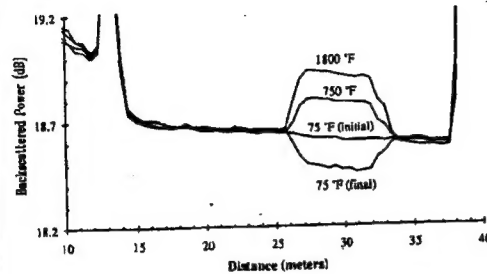
**Parameter:**

- Laser: 514nm Lexel 3000 Argon-Ton laser
- Laser linewidth: 3MHz
- Fiber type: Birefringent fiber
- Core diameter: 2  $\mu\text{m}$
- Beat length: 1mm

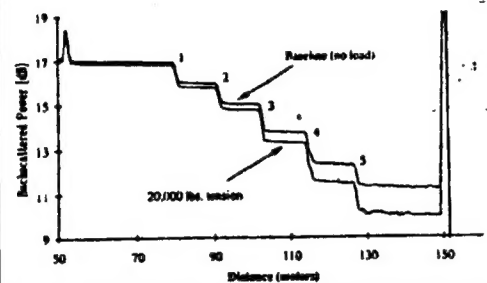




1. OTDR traces of 50/125μm graded index fiber at 840nm wavelength. 100 meter fiber segment in oven. Upper trace, 1100°F. Lower trace, cooling to 127°F.



2. OTDR traces of 50/125μm graded index fiber showing irreversible change after cycling fiber to 1800°F. Note (in the lower trace) the return to the same level of scattering after the heated up region as before, indicating no extra attenuation associated with the irreversible change.



3. OTDR response of optical fiber embedded aluminum lap jointt showing sensing response from all five sensing fiber passes under tension. The loss steps at zero load were purposely introduced to "prebias" the sensors. Note the effect of the cumulative response from each sensing fiber pass.

Table 2

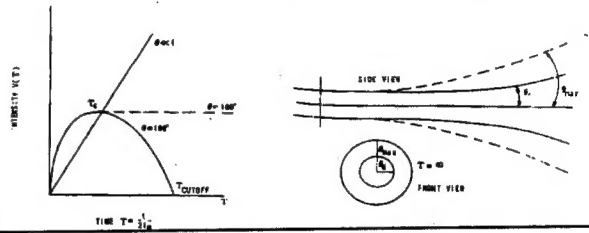
| Bragg Condition $f_B = (f_B)_\pi \sin \frac{\theta}{2}$ |   |
|---|---|
| References  | <div>sBs (<math>\theta = \pi \pm \delta\theta</math>)</div> <div>GAWBS (<math>\theta = 0^\circ \pm \delta\theta</math>)</div>   |
| Stone J. (1983)   | <div>Fused quartz: <math>(f_B)_\pi = 12.6\text{GHz}</math> at <math>\lambda = 1.3\mu\text{m}</math>, <math>\delta\theta = \lambda/\pi n a \approx 0.08</math></div> <div>Linewidth:<br/> <math>\delta f_B = \frac{1}{4}(f_B)_\pi (\delta\theta)^2 \ll 100\text{MHz}</math> </div>   |
| Jen C.K. (1989)   | <div>Linewidth:<br/> <math>\delta f_B = \frac{1}{2}(f_B)_\pi \delta\theta \approx 500\text{MHz}</math> </div> <div> <math>\frac{dA_i(z)}{dz} = -jC^*(z)A_d(z)</math><br/> <math>-\frac{dA_d(z)}{dz} = -jC(z)A_i(z)</math><br/>           where <math>A_i</math> and <math>A_d</math> are amplitudes of incident and diffracted optical waves, respectively.<br/> <math>C = C^i + C^x + C^\pi + C^{\pi\phi} + C^{\phi x}</math><br/> <math>C^x, C^{\pi\phi}, C^{\phi x} \ll C^i, C^\pi, C^{\pi\phi} \approx 5\% C^i</math><br/> <math>C^i</math> for <math>L_{01} = \text{sBs}</math> dominates (<math>L_{0m}, L_{2m}</math>)         </div> <div> <math>C^i = b \int (E_r^* \Delta \epsilon_{rr} E_r + E_\phi^* \Delta \epsilon_{\phi\phi} E_\phi) r dr d\phi</math><br/> <math>C^x = b \int E_z^* \Delta \epsilon_{zz} E_z r dr d\phi</math><br/> <math>C^\pi = b \int E_z^* \Delta \epsilon_{zz} E_r r dr d\phi</math><br/> <math>C^{\pi\phi} = b \int E_r^* \Delta \epsilon_{r\phi} E_\phi r dr d\phi</math><br/> <math>C^{\phi x} = b \int E_\phi^* \Delta \epsilon_{\phi z} E_z r dr d\phi</math><br/>           where <math>b = \omega_0 \epsilon_0 / 4</math> </div> <div> <math>\Delta \epsilon_{rr} = q [p_{11}(r) S_{rr} + p_{12}(r) S_{\phi\phi} + p_{12}(r) S_{zz}]</math><br/> <math>\Delta \epsilon_{\phi\phi} = q [p_{12}(r) S_{rr} + p_{11}(r) S_{\phi\phi} + p_{12}(r) S_{zz}]</math><br/> <math>\Delta \epsilon_{zz} = q [p_{12}(r) S_{rr} + p_{12}(r) S_{\phi\phi} + p_{11}(r) S_{zz}]</math><br/> <math>\Delta \epsilon_{rz} = 2qp_{44} S_{rz}</math><br/> <math>\Delta \epsilon_{r\phi} = 2qp_{44} S_{r\phi}</math><br/> <math>\Delta \epsilon_{\phi z} = 2qp_{44} S_{\phi z}</math><br/>           where <math>q = -n^4(r)</math> </div> <div> <math>S_{rr}, S_{\phi\phi}, S_{zz} \propto \cos n\phi</math>    <math>S_{r\phi}, S_{\phi z} \propto \sin n\phi</math><br/>           for <math>\text{HE}_{11}</math>: <math>E_r \propto \cos \phi</math>, <math>E_\phi \propto \sin \phi</math>, <math>E_z \propto \cos \phi</math><br/> <math>\therefore c=0</math>, except for <math>n=0, 2</math> only <math>F_{2m}, +R_{0m}, = TR_{2m}</math> </div> |
| Marcuse D. (1991)                                       | <div>Predicted depolarization of incident laser light in the fiber by periodic variation in the fiber diameter causing birefringence in the fiber.</div> <div> <math>r = a_0 + f \sin 2\phi</math><br/> <math>K_{00} = -i \frac{f K^2 \gamma^2}{4n_1 a_0 k \beta^2} F</math>    <math>F = 1 + \left(1 - \frac{\gamma^2}{K^2}\right) \frac{J_0^2(Ka_0)}{J_1^2(Ka_0)} + \frac{(\gamma a_0)^2 J_0^3(Ka_0)}{Ka_0 J_1^3(Ka_0)}</math><br/> <math>\frac{f A^{3/2}}{a_0^2} L_p = \frac{\pi V^3}{\sqrt{2}(Ka)^2 (\gamma a)^2 F} = 2.5</math><br/> <math>L_p</math> is the length required for the polarization to rotate by <math>90^\circ</math><br/> <math>a_0 = 5\mu\text{m}</math>, <math>\Delta = 0.00137</math>, <math>V = 2.4</math><br/>           For <math>f = 0.05\mu\text{m}</math> (1% elliptically), <math>L_p = 25\text{m}</math> </div>   |
| Corvo A. (1988)   | <div>Concluded theoretically that GAWBS would dominate over sBs for long pulse or cw lasers, and also correctly predicted the frequency shift increase with increasing diffraction angle.</div> <div>  </div>   |
| Shelby R.M. (1985)                                      | <div>First group to predict GAWBS.</div> <div> <math>TR_{2m}</math> modes (<math>q_{  } \approx 0</math>)<br/>           Light propagating with linear polarization at <math>\phi = 45^\circ</math> encounter anisotropic perturbations which cause unequal phase shifts for components projected on the <math>\phi = 0^\circ</math> and <math>\phi = 90^\circ</math> axes. Polarization components are created along <math>\phi = 45^\circ</math> that are frequency up shifted and down shifted by the vibrational mode. The fraction depolarized in this way by the index perturbations is<br/> <math display="block">\eta_f = \frac{n^6 \omega^2 k T (A_1 - \alpha^2 A_2)^2 (P_{11} - P_{12})^2}{64 \pi c^2 \rho V_s^2 a^2 B_{7m}} \approx 10^{-12} \text{ cm}^{-1} \text{ for } TR_{25} \text{ mode}</math><br/>           The frequency shift <math>f_m</math> of the light wave scattered due to <math>TR_{2m}</math> modes is expressed as<br/> <math display="block">f_m = \frac{V_s y_m}{\pi d}</math><br/>           where <math>V_s</math> denotes the sound velocity of the shear wave and <math>d</math> is the fiber diameter. <math>y_m</math> is the eigenvalue related to the frequency <math>f_m</math> of the light scattered by <math>TR_{2m}</math> mode and is obtained by solving the following equation, which is determined by boundary conditions for <math>TR_{2m}</math> modes corresponding to zero traction on the fiber surface,<br/> <math display="block">\begin{vmatrix} \left(3 - \frac{y_m^2}{2}\right) J_2(\alpha y_m) &amp; \left(6 - \frac{y_m^2}{2}\right) J_2(y_m) - 3y_m J_3(y_m) \\ J_2(\alpha y_m) - \alpha y_m J_3(\alpha y_m) &amp; \left(2 - \frac{y_m^2}{2}\right) J_2(y_m) + y_m J_3(y_m) \end{vmatrix} = 0</math> </div>   |

Table 3 Available GAWBS experimental data

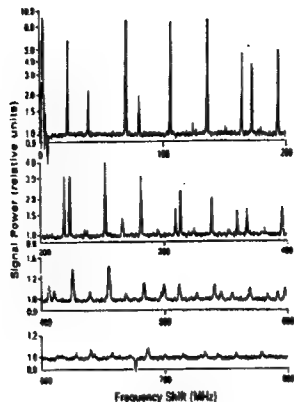
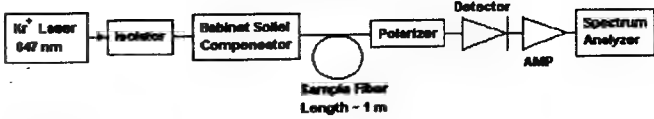
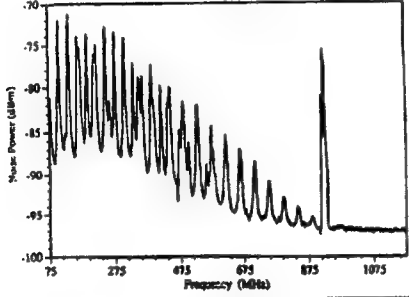
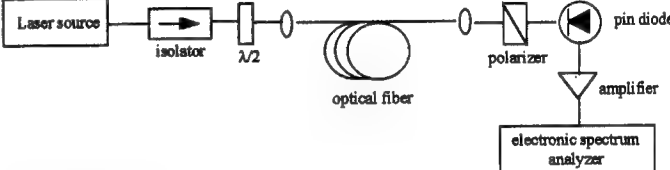
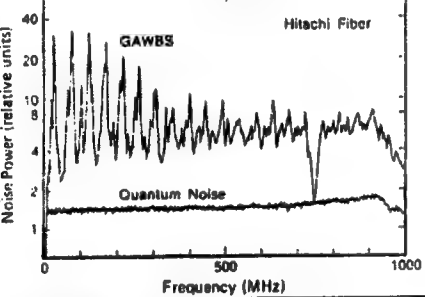
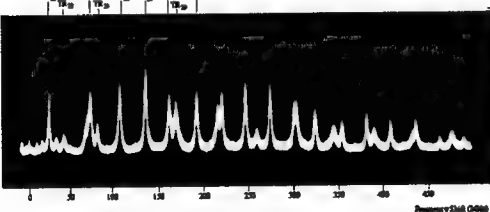
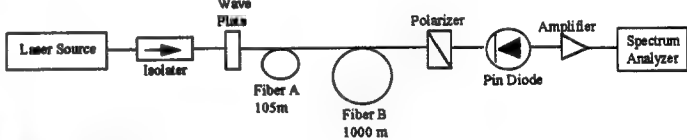
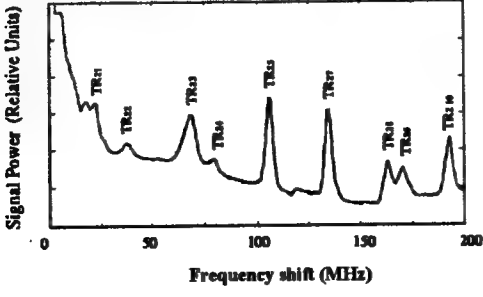

| Reference              | GAWBS  | Experimental Setup  |
|------------------------|--|---|
| (a) Shelby R.M. (1985) |   |  <p><b>Parameters:</b></p> <ul style="list-style-type: none"> <li>- Laser: 647nm Kr<sup>+</sup> Spectra-Physics laser</li> <li>- Fiber Length: 1m singlemode fiber</li> <li>- Core: 4±0.4μm germania-doped silica</li> <li>- Cladding: 125±3μm pure synthetic silica</li> <li>- Input power: 200mW</li> <li>- Output power: 1-5mW</li> <li>- Pump linewidth: few MHz</li> </ul> |
| (b) Poustie (1992)     |   |  <p><b>Parameters:</b></p> <ul style="list-style-type: none"> <li>- Laser: 1321nm 50 mW CW multimode Nd:YLF laser</li> <li>- Fiber length: 4000m standard telecommunication fiber</li> </ul>  |
| (c) Perlmutter (1990)  |                                        | <p><b>Parameters:</b></p> <ul style="list-style-type: none"> <li>- Fiber length: 100 m</li> <li>- Fiber type : Single-mode fused-silica optical fiber</li> <li>- Fiber core: ~ 5 μm</li> <li>- Fiber cladding: ~ 125 μm</li> </ul>  |
| (d) Yu (1994)          | <p>GAWBS spectrum for test fiber</p>  |  <p><b>Parameters:</b></p> <ul style="list-style-type: none"> <li>- Laser: 1319nm Nd:YAG ring laser</li> <li>- Laser linewidth: &lt; 10kHz</li> <li>- Fiber type : "Z" fiber from LITESPEC Inc</li> <li>- Fiber length: 1000 m.</li> </ul>  |
| (e) Shiraki K. (1992)  | <p>GAWBS spectrum</p>                 |  <p><b>Parameters:</b></p> <ul style="list-style-type: none"> <li>- Laser: 1550nm DFB laser</li> <li>- Fiber length: 3000m</li> <li>- Core: 5μm pure silica</li> <li>- Cladding: 126±0.3μm ( F-doped silica)</li> <li>- Input power: 2mW</li> <li>- Pump linewidth: &lt;200 kHz</li> </ul>  |

Table 4       $TR_{2m}$  Mode Intensity Chart (Yu)

| Mode       | Intensity   |
|------------|-------------|
| $TR_{21}$  | strong      |
| $TR_{22}$  | weak        |
| $TR_{23}$  | strong      |
| $TR_{24}$  | weak        |
| $TR_{25}$  | very strong |
| $TR_{26}$  | almost zero |
| $TR_{27}$  | very strong |
| $TR_{28}$  | strong      |
| $TR_{29}$  | strong      |
| $TR_{210}$ | strong      |

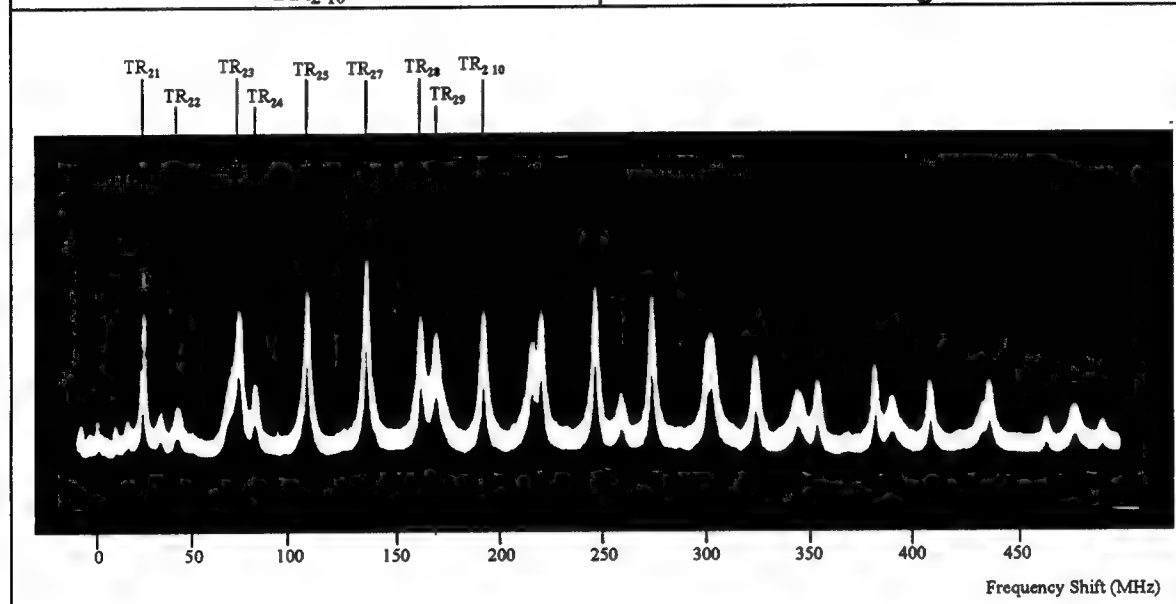
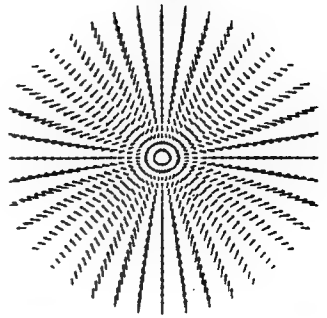
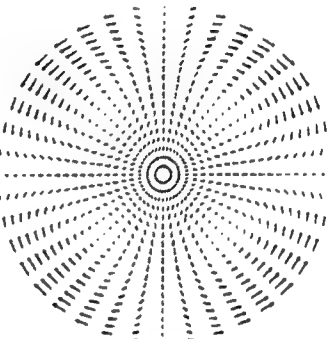
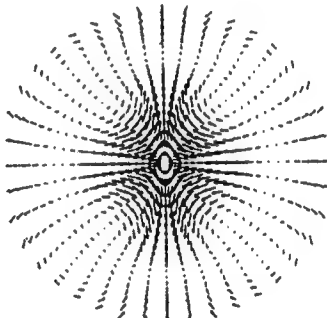
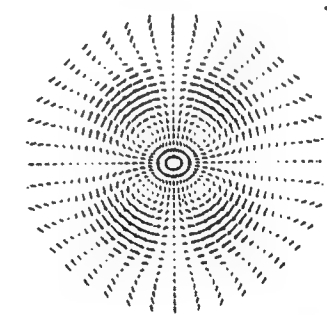
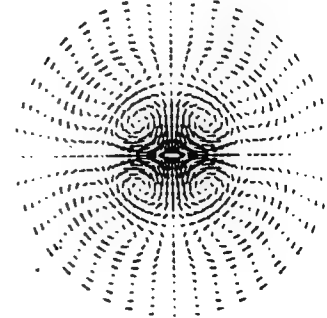


Table 5  $TR_{2m}$  Mode Birefringence Chart

| Mode      | Birefringence | Arrow Plot  |
|-----------|---------------|---|
| $TR_{21}$ | HiBi          |    |
| $TR_{22}$ | LoBi          |    |
| $TR_{23}$ | HiBi          |   |
| $TR_{24}$ | LoBi          |  |
| $TR_{25}$ | Strong HiBi   |  |

TR<sub>2m</sub> Mode Birefringence Chart (Cont.)

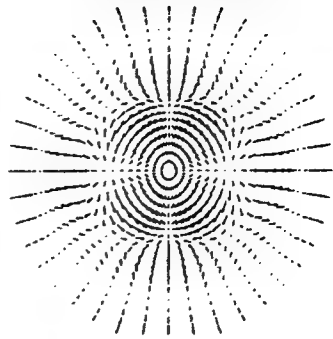
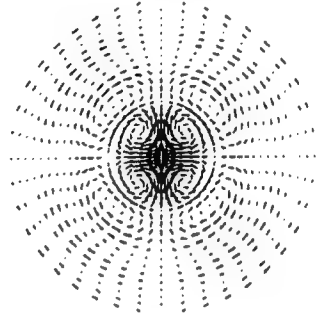
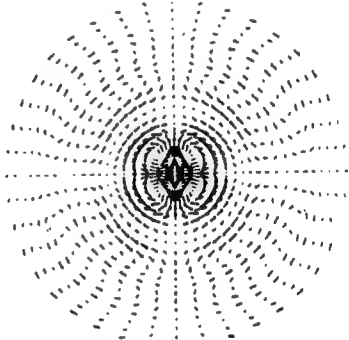
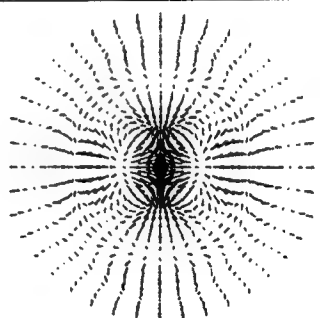
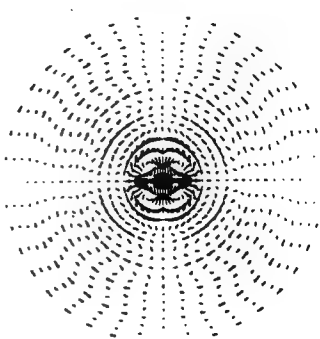
| Mode               | Birefringence | Arrow Plot  |
|--------------------|---------------|---|
| TR <sub>26</sub>   | Zero Bi       |    |
| TR <sub>27</sub>   | Strong Bi     |    |
| TR <sub>28</sub>   | HiBi          |   |
| TR <sub>29</sub>   | HiBi          |  |
| TR <sub>2 10</sub> | HiBi          |  |

Table 6 Maximum GAWBS Bandwidth Calculation and Observation

| Reference  | Pump Wavelength     | Core radius       | $\delta\theta = \lambda / \pi n a$<br>$n=1.46$ | $(f_B)_\pi$<br>(GHz) | Observed $(\delta f_B)_\pi$<br>(MHz) | $(\delta f_B)_\pi = (f_B)_\pi \times \delta\theta / 2$<br>(MHz) |
|------------|---------------------|-------------------|--|----------------------|--------------------------------------|---|
| Stone      | 1.3 $\mu\text{m}$   | 3.5 $\mu\text{m}$ | 0.08   | 12.7                 | —                                    | 500   |
| Shelby     | 0.647 $\mu\text{m}$ | 2.0 $\mu\text{m}$ | 0.0686   | 26.5                 | 800                                  | 910   |
| Shiraki    | 1.55 $\mu\text{m}$  | 2.5 $\mu\text{m}$ | 0.135  | 11.3                 | —                                    | 764   |
| Yu         | 1.319 $\mu\text{m}$ | 4.9 $\mu\text{m}$ | 0.0587   | 13.2                 | 400                                  | 387   |
| Perlmutter | 0.647 $\mu\text{m}$ | 2.5 $\mu\text{m}$ | 0.0564   | 26.5                 | 900                                  | 748   |
| Poustie    | 1.321 $\mu\text{m}$ | —                 | —  | —                    | 875                                  | —   |

\* Index of refraction varies widely, so that  $(f_B)_\pi$  is only approximate.

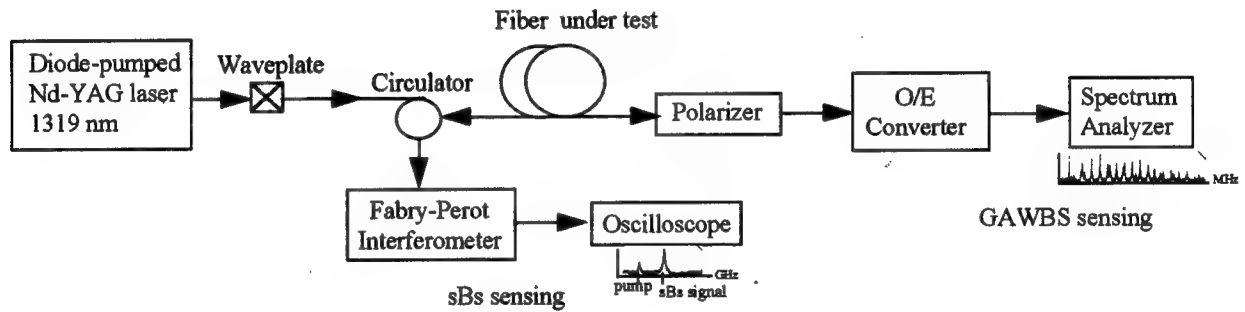
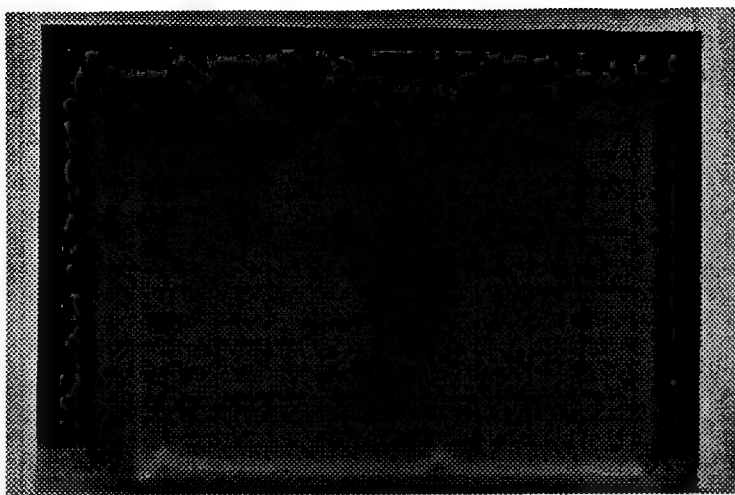
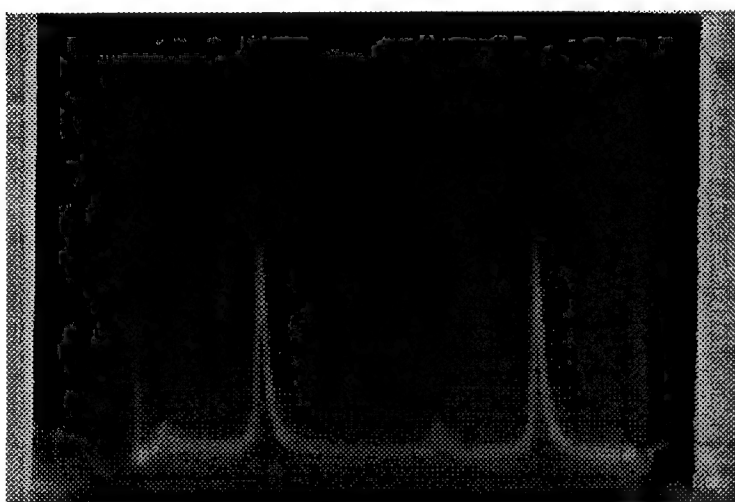


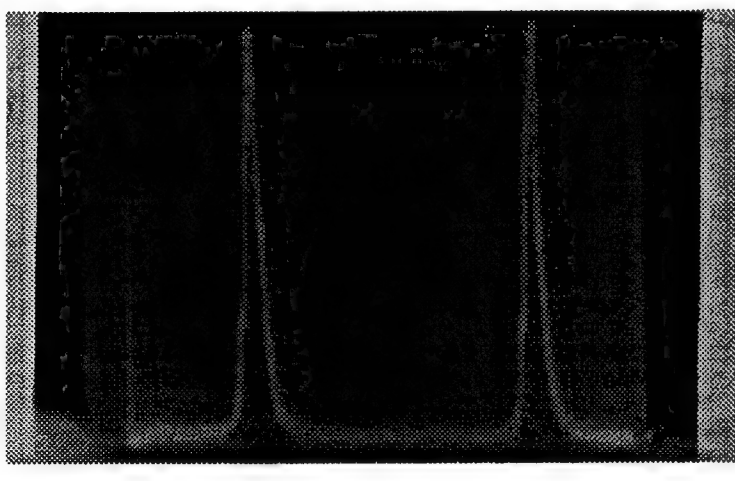
Fig.1 Setup for Dual Sensing



No fiber spectrum of pump  
cross talk



1000 m fiber sBs signal



3000 m fiber sBs signal

Laser pump = 72.5 mW

Fig.2 SBr signal from different fiber lengths



## **2. GAWBS BASED FIBER SENSOR PRELIMINARY TESTS**

1 km of single-mode fiber was bonded to a plexiglass plate, which was then mounted on a vibration table as shown in Table 7 (a). Vibration frequencies ranges from 0 - 5000 Hz, and vibration amplitude could also be varied.

In part (b) of Table 7, four holes were drilled in the plexiglass plate. The plate was then mounted and vibrated in a range of frequencies. At 100 Hz, the GAWBS spectrum was maximally distorted, and we identified this as the resonance frequency of the plate with 4 drilled holes.

Four additional holes were drilled as shown in part (c) of Table 7. The GAWBS spectrum was again mounted as the vibration frequency was swept. Resonant frequencies were recorded at 100 Hz, 200 Hz and 300 Hz.

It is clear from these experiments that the GAWBS spectrum is sensitive to structural variations (cracks or holes).

To verify the prediction of Table 8 as to the temperature insensitivity of the GAWBS spectrum, a preliminary experiment was conducted by raising the ambient temperature of the fiber from 0°C to 58°C. The setup is shown in Table 9. A short fiber segment was bonded to a plastic plate and the GAWBS spectrum monitored as the plate was cooled and heated. The GAWBS spectrum did not exhibit noticeable shift or amplitude variations.

One of the key factors in structural degradation is corrosion. Thus, corrosion detection is an essential part of a structural sensor. One set of experiments were carried out by us to ascertain the capability of the GAWBS sensor in sensing chemical composition variation is the fiber cladding. 1 km of pure silica core Sumitomo Z-fiber was connected to 105 m of Sumitomo Ge-doped G-fiber. GAWBS spectra of the Z-fiber alone and Z-G combined fiber were recorded and compared. The result is shown in Table 10 (a). For higher order modes, the additional mode peaks due to the short (105 m) G-fiber are clearly visible. Thus, chemical contamination of the fiber, such as that due to corrosion, should be detectable in the GAWBS spectrum.

Shiraki has demonstrated in Table 10 (b), that fiber diameter variations are detectable in the GAWBS spectrum. In his case, two equal length fiber segments (3 km) of different diameter s were used, thus, yielding more peaks of equal strengths. We are proceeding to modify this setup

by having shorter fiber lengths and also of significantly different lengths to observe the detectability of fiber diameter variations by the GAWBS spectrum. These results are expected to translate into sensing application for fiber mechanical perturbations.

Table 7 GAWBS Based Fiber Sensor Jig Mounted on Vibration Table


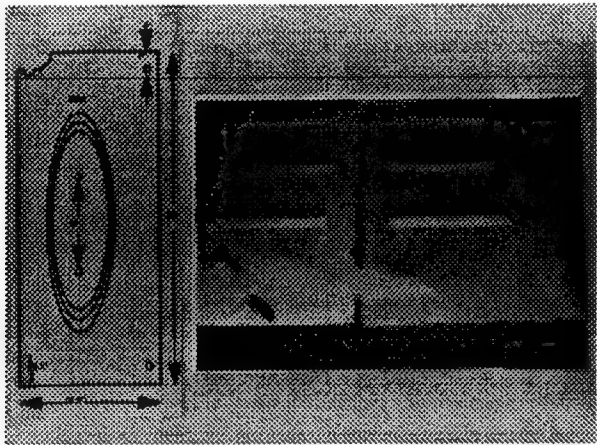

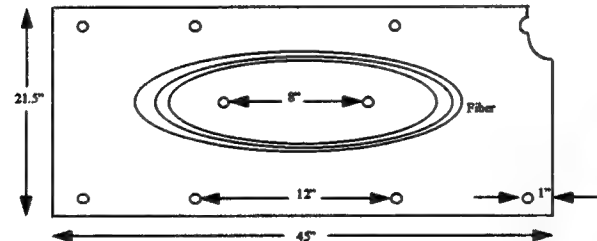
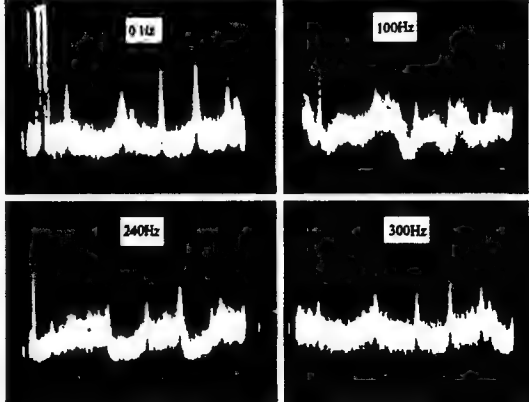
| Parameters   | Experimental Setup  | Test Results   |
|--|---|--|
| (a)<br>1000 m single-mode fiber test coupon mounted on the vibrating table |    |  |
| (b)<br>Test jig with 4 drilled holes at 4 corners                          |   | GAWBS vibration spectrum. Resonance at 100 Hz<br>  |
| (c)<br>Test jig with 8 drilled holes                                       |  | GAWBS vibration spectrum at various vibration frequencies. Resonances exhibit at 100, 200, 300 Hz when GAWBS spectra undergo maximum vibrations<br> |

Table 8 Calculation of GAWBS Temperature Dependence

| Reference  | Temperature Range,<br>$\Delta T$ | SBS Shift<br>$\Delta(f_B)_\pi$ | Max. GAWBS Shift,<br>$\Delta(\delta f_B) = 1/2 \Delta(f_B)_\pi \delta \theta$ |
|--|----------------------------------|--------------------------------|---|
| Bao  | 90°C - 10°C = 80°C               | 40 MHz                         | 1.6 MHz   |
| Kurashima  | 60°C - (-30°C) = 90°C            | 112.5 MHz                      | 4.5 MHz   |
| <b>Conclusion:</b> GAWBS spectrum is independent of ambient temperature, since max. $\Delta(\delta f_B)$ < 5 MHz, which is not resolvable in the GAWBS spectrum (of 20 MHz scale). |                                  |                                |   |

Table 9 Test Jig for Ambient Temperature Variation

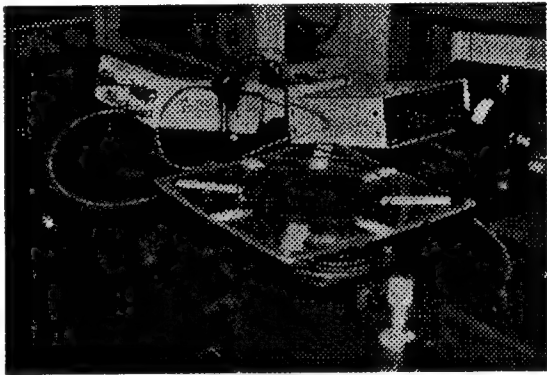
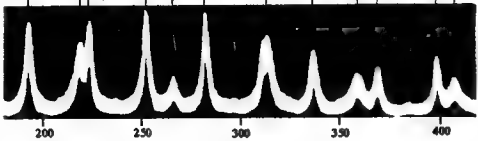

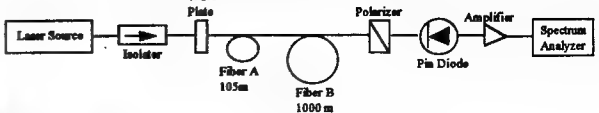
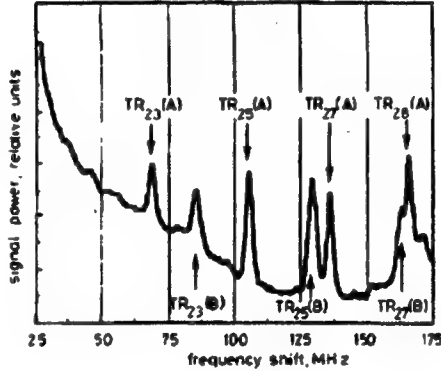
| Parameters  | Experimental Setup  | Test Results  |
|---|---|---|
| Fiber length: 12 m<br>Laser Power: 145 mW<br>Heater: BroilKing portable stove |  | <u>Mode Amplitude</u><br>- No change<br><br><u>Mode Frequency</u><br>- No shift |

Table 10

| Reference                | GAWBS  | Experimental Setup  |
|--------------------------|--|---|
| (a) Yu<br>(1994)         | <p>GAWBS spectrum for fiber B</p>  <p>GAWBS spectrum for fibers A+B</p>  |  <p><b>Parameter</b></p> <ul style="list-style-type: none"> <li>- Laser: 1319 nm Nd:YAG ring laser</li> <li>- Laser linewidth: &lt; 10 kHz</li> <li>- Fiber type : A: "G" fiber from Sumitomo<br/>B: "Z" fiber from Sumitomo</li> <li>- Fiber length: A: 105 m<br/>B: 1000 m</li> </ul>                                   |
| (b) Shiraki K.<br>(1992) |    | <p>GAWBS spectrum shift with fiber diameter.<br/>Setup similar to (a).</p> <p><b>Fiber Parameters</b></p> <ul style="list-style-type: none"> <li>- Length: 3000 m</li> <li>- Core: Pure silica</li> <li>- Cladding: 1.08 wt% F-doped silica cladding</li> <li>- Fiber A: Outer diameter = 125 <math>\mu\text{m}</math></li> <li>- Fiber B: Outer diameter = <math>\approx 100 \mu\text{m}</math></li> </ul> |

## RESULTS OF PRELIMINARY STUDY

1. The GAWBS spectrum as reported by various groups has been compiled and repeatedly confirmed by us experimentally;
2. The sBs Stokes shift as reported by many groups has been experimentally confirmed by us in varying fiber lengths and incident laser power levels;
3. Various theoretical models of the GAWBS phenomenon, have been compiled, compared and reconciled with the basic sBs phenomenon, obeying the same Bragg condition;
4. SBS as a temperature and strain sensor has been examined. Its limitation of long fiber length and high laser power requirements is noted. Simultaneous temperature and strain induced sBs shift may render single-measurand sensing impossible;
5. The superiority of the GAWBS sensing mechanism in terms of short fiber length, low laser power as compared to those required by sBs has been theoretically confirmed. Its temperature independence is indicated and experimentally confirmed. This feature may enable GAWBS as a purely structural sensor;
6. Various singlemode fiber lengths have been bonded to plastic plates to simulate to some extent flexible aircraft structures. These plates were mounted on a variable-frequency vibration jig, and subject to mechanical vibrations of varying amplitudes and frequencies. Resonant frequencies were recorded when the GAWBS spectrum exhibited maximum mode amplitude variations. Additional holes were drilled in the plastic plates to simulate cracks and the same vibration tests repeated. Different resonant frequencies were resonant frequencies were recorded. Such resonances were very sharp, to within 1 Hz;

7. The free standing singlemode fiber depolarizes light very readily. However, when bonded to the plastic structure, such depolarization was found to be minimal;
8. It appears that the GAWBS spectrum shifts readily with fiber diameter and doping variations. This is an excellent indication of the sensing potential of this spectrum for corrosion and strain in the fiber, and hence those of the structure to which the fiber is bonded.

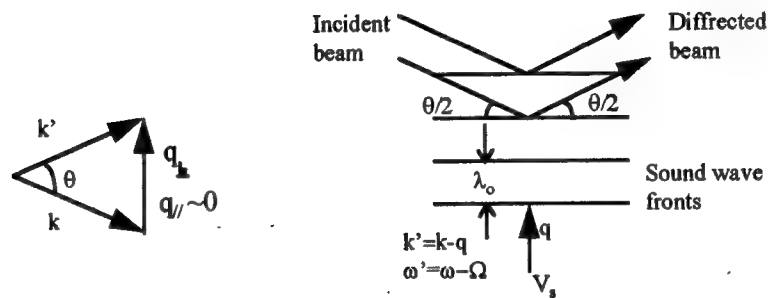
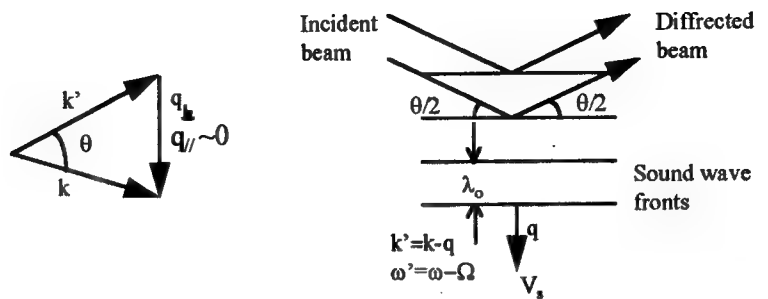
### 3. REFERENCES

- J.Stone, and A.R.Chraplyvy, "Spontaneous Brillouin Noise In Long-Distance High-Bandwidth Optical-Fiber Transmission", *Electronics Letters*, Vol.19, No.8, 14th April 1983, p.275-276.
- C.K.Jen, and N.Goto, "Backward Collinear Guided-Wave-Acousto-Optic Interactions In Single-Mode Fibers", *Journal of Lightwave Technology*, Vol. 7, No.12, December 1989, p. 2018-2023.
- D.Marcuse, "Theory of Dielectric Optical Waveguides", *Academic Press, Inc.*, 1991, p.135-176.
- A.Corvo, and A.Gavrielides, "Forward Stimulated Brillouin Scattering", *Journal of Applied Physics*, Vol.63, No.11, 1st June 1988, p.5220-5227.
- R.M.Shelby, M.D.Levenson, and P.W.Bayer, "Guided Acoustic-Wave Brillouin Scattering", *Physical Review B*, Vol.31, No.8, 15th April 1985, p.5244-5252.
- K.Shiraki, and M.Ohashi, "Sound Velocity Measurement Based on Guided Acoustic-Wave Brillouin Scattering", *IEEE Photonics-Technology Letters*, Vol.4, No.10, October 1992, p.1177-1180
- M.Ohashi, N.Shibata and K.Shiraki, "Fiber Diameter Estimation Based On Guided Acoustic Wave Brillouin Scattering", *Electronics Letters*, Vol.28, No.10, May 1992, p.900-902.
- X.Bao, D.J.Webb, and D.A.Jackson, "Combined Distributed Temperature and Strain Sensor Based On Brillouin Loss In An Optical Fiber", *Optics Letters*, Vol.19, No.2, 15th January 1994, p.141-143.
- T.Kurashima, T.Horiguchi, and M.Tateda, "Distributed-temperature Sensing Using Stimulated Brillouin Scattering In Optical Silica Fibers", *Optics Letters*, Vol.15, No.18, 15th September 1990, p.1038-1040.
- C.J.Duffy, and R.P.Tatam, "Optical Frequency Shifter Technique Based On Stimulated Brillouin Scattering In Birefringent Optical Fiber", *SPIE Vol.1511 Fiber Optic Sensors: Engineering and Application (1991)*. p.155-165.
- P.B.Ruffin, and C.C.Sung, "Sensitivity of Polarization-maintaining Fibers to Temperature Variations", *SPIE Vol.1478 Sensors and Sensor Systems for Guidance and Navigation (1991)*, p.160-167.



# 4. APPENDIX

## GAWBS



## SBS

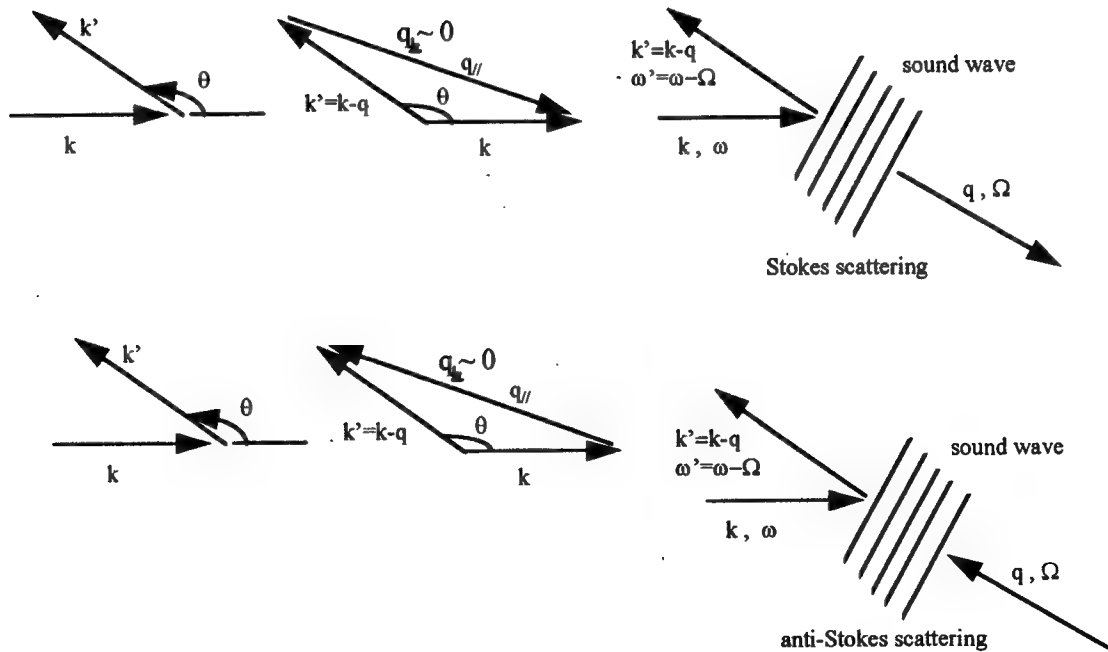


Fig.1

$$\Omega = 2|k|v \sin(\theta/2) = 2n\omega v/c \sin(\theta/2)$$

The vibrational modes of a cylinder are characterized by a transverse displacement profile and a wave vector in the direction parallel to the cylinder axis. The transverse profile can be classified according to the character of their motion as torsional, radial, longitudinal, flexural, or mixtures of these motions. The modes responsible for forward scattering light in the core are radial modes independent of  $\phi$  ( $R_{0m}$ ) or mixed torsional-radial modes varying sinusoidally as  $2\phi$  ( $TR_{2m}$ ), the latter being doubly degenerate. A nearly infinite number of modes and a similar number of nonzero mode frequencies exists for each value of the axial wave vector  $q_{||}$ . This multiplicity of dispersion curves is the key difference between the bulk sBs scattering case and scattering considered here by guided acoustic-wave in an optical fiber. The frequencies detected correspond to axial wave vectors near  $q_{||}=0$ .

Polarized scattering results from the radial dilatation or  $R_{0m}$  modes which cause pure phase modulation. To detect this effect, a single-mode fiber must be used as one arm of a Mach-Zehnder interferometer. To detect depolarized scattering which is due to the  $TR_{2m}$  modes, elliptically polarized light is coupled into the fiber core under conditions where the polarization of the output is identical to the input as in polarization maintaining fibers. A Glan-Thompson polarizer after the fiber rejects the linear polarization corresponding to the major axis of the input. The much weaker minor-axis polarization is directed onto the photodiode and acts as a local oscillator in heterodyne detection of the depolarized scattering of light initially polarized along the major axis.

In a uniform cylinder, the frequencies of these mode depend only on cylinder radius,  $a$ , velocity of the longitudinal (dilation  $R_{0m}$ ) modes,  $V_d$ , velocity of the mixed torsional-radial or transverse (shear,  $TR_{2m}$ ) modes,  $V_s$ , and the wave vector along the cylinder axis. Each mode couples the incident and a forward scattered photon, thus giving rise to a Stokes and an anti-Stokes peak in the light scattering spectrum for each mode.

For polarized guided Brillouin spectrum of  $R_{0m}$  modes in a single mode fiber:

Scattering efficiency

$$\eta_F = \frac{n^6 \omega^2 k T (P_{11} + P_{12})^2}{32 \pi c^2 \rho V_d^2 a^2 B_{Rm}}$$

$$B_{Rm} = \int_0^2 J_1^2(y_m x) x dx$$

$P_{11}=0.121$ ,  $P_{12}=0.270$  are the strain-optic coefficient for fused quartz

$n$  is index of reflection

For the strong  $R_{03}$  mode at 127 MHz,  $n_F = 4.4 \times 10^{-12} \text{ cm}^{-1}$

For depolarized guided Brillouin scattering spectrum of  $TR_{2m}$  modes in a single-mode fiber:

Scattering efficiency

$$A_1 = (6 - y_m^2) J_2(\alpha y_m)$$

$$A_2 = (6 - y^2/2) J_2(y_m) - 3 y_m J_3(y_m)$$

$B_{Tm}$  is analogous to  $B_{Rm}$

$$\eta_F = \frac{n^6 \omega^2 k T (A_1 - \alpha^2 A_2)^2 (P_{11} - P_{12})^2}{64 \pi c^2 \rho V_s^2 a^2 B_{Tm}}$$

$$\eta = 1.4 \times 10^{-12} \text{ cm}^{-1} \text{ for } TR_{25}$$

$\Omega_m = (V_d y_m)/a$  gives the frequency  $m$ th  $R_{0m}$  mode

$y_m$  is the  $m$ th zero of the Bessel function

For fused silica,  $V_s = 3740 \text{ m/sec}$  and  $V_d = 5996 \text{ m/sec}$

$$\Omega_m = V_s y_m/a \text{ for } TR_{2m} \text{ mode}$$

Modes with  $q_{||} = 4\pi n/\lambda$  cause backscattering of the incident radiation with a frequency shift of  $\Omega_m \approx 4\pi n V_d/\lambda$ . The linewidth of the observed backward Brillouin scattering is roughly 145 MHz in a fiber. On the basis of the above analysis, a pattern of splittings similar to that due to forward scattering should be detectable in the backscattering case. This light scattering phenomenon constitutes a thermal-noise source within all optical fibers and might ultimately be significant in communications and sensor applications of these devices.

## ACOUSTIC COUPLING TO OPTICAL FIBERS

When a plane acoustic wave is incident on an optical fiber, modeled as an infinite cylinder, the pressure in the interior of the fiber is a function of the ratio of radius to the acoustic wavelength. When this ratio is small the pressure is transmitted to the fiber interior without reflection loss, as predicted below.

For a plane wave of sound incident normally to the axis of a fiber is of radius  $a$ , density  $\rho_0$ , speed of sound  $c_0$ , and of the form

$$p = p_0 e^{i(kx - \omega t)} = p_0 e^{i(k\gamma \cos \phi - \omega t)}$$

where  $p_0$  is the amplitude of the pressure disturbance,  $\omega$  is the sound frequency,  $k$  is the wave number,  $\gamma$  is the radial vector in cylindrical coordinates, and  $\phi$  is the angle between the radial vector and the direction of the incident acoustic wave, the solution is

$r < a$ :

$$p = p_0 \sum_{m=0}^{\infty} \epsilon_m i^m B_m \cos m\Phi J_m \left( \frac{c}{c_0} k\gamma \right)$$

$r > a$ :

$$p = p_0 \sum \epsilon_m i^m \cos m\Phi [J_m(k\gamma) + D_m H_m^1(K\gamma)]$$

Hence  $\epsilon_m = 1$ ,  $m=0$ ,  $\epsilon_m = 2$ ,  $m>0$ ,  $\phi$  is the azimuthal angle,  $J_m$  is the  $m$ th-order Bessel function and  $H_m^1$  is the  $m$ th-order Hankel function of the first kind. We then find the radial velocity from

$$v = \frac{1}{i\rho\omega} \nabla p$$

and require that the pressure and radial velocity be continuous at  $\gamma=a$ . After eliminating  $D_m$ , we arrive at

$$B_o = \frac{1 + \left(\frac{1}{2}ka\right)^2}{1 + \left(\frac{1}{2}ka\right)^2 - 2\left(1 - \frac{\rho c^2}{\rho_e c_e^2}\right) \left(\log \frac{1}{2}ka + \gamma\right) \left(\frac{1}{2}ka\right)^2}$$

where  $\gamma$  = Euler's constant = 0.577 .....

Since  $ka = 2\pi a/\lambda$ , where  $\lambda$  is the acoustic wavelength, we have

$$\lim_{a/\lambda \rightarrow 0} B_o =$$

For  $m > 0$ ,  $B_m$  vanishes at least as fast as  $B_o$  and, in addition, is multiplied by the factor  $J_m[(c/c_e)k\gamma]$  which, for  $\gamma < a$ ,  $c_e > c$  is much less than unity. Thus for acoustic wavelengths long compared to the fiber radius the sound is completely coupled to the fiber interior.